Three-Dimensional Simple Adjoint Velocity Retrievals from Single-Doppler Radar

JIDONG GAO AND MING XUE

Center for Analysis and Prediction of Storms, University of Oklahoma, Norman, Oklahoma

ALAN SHAPIRO

Center for Analysis and Prediction of Storms, School of Meteorology, Coastal Meteorology Research Program, University of Oklahoma, Norman, Oklahoma

QIN XU

National Severe Storms Laboratory, Norman, Oklahoma

KELVIN K. DROEGEMEIER

Center for Analysis and Prediction of Storms, School of Meteorology, University of Oklahoma, Norman, Oklahoma

(Manuscript received 22 November 1999, in final form 21 March 2000)

ABSTRACT

In this paper, the original simple adjoint method of Qiu and Xu is improved and tested for retrieving the 3D storm-scale wind field from single-Doppler radar data. The method incorporates single-radar data and background fields, along with a dynamical constraint, smoothness, and anelastic mass continuity constraint, in a cost function. The minimization of the cost function, with the desired fit to these constraints, is obtained in an iterative procedure.

The current method is tested on simulated datasets of supercell storms. It is shown that the circulation inside and around the storms, including the strong updraft and associated downdraft, are well retrieved. Furthermore, the method is robust in the presence of data error.

1. Introduction

Doppler radar has long been a valuable observational tool in meteorology. It has the capability of observing, at high spatial and temporal resolution, the internal structure of storm systems from remote locations. However, direct measurements are limited to reflectivity, the radial component of velocity, and the spectrum width; there is no direct measurement of the complete three-dimensional (3D) wind field. In order to gain a more complete understanding of the atmosphere, as well as initialize storm-resolving numerical models, it is necessary to know the full 3D wind field.

Since the early study of Rinehart (1979), techniques for retrieving the unobserved wind components from single-Doppler radial velocity and perhaps reflectivity data have been developed (Tuttle and Foote 1990; Sun et al. 1991; Liou et al. 1991; Qiu and Xu 1992; Sun and Crook 1997, 1998; Shapiro et al. 1995; Laroche and Zawadski 1994; Weygandt et al. 1995; Zhang and Gal-Chen 1996). Detailed reviews of these and other methods can be found in Shapiro (1995).

The so-called simple adjoint (SA) method was first explored and tested with simulated data by Qiu and Xu (1992, henceforth referred to as QX92). It was then upgraded and tested using Phoenix II data by Xu and Qiu (1994) and Xu et al. (1994a), and further tested with Denver microburst data by Xu and Qiu (1995). As demonstrated in these studies, the most important features of the SA method can be summarized as follows. (i) It uses the observed reflectivity (and/or radial wind) as a tracer in the reflectivity advection equation (and/or radial wind) to retrieve the time mean (or running mean) wind field averaged over several time levels of radar scans; by using data gathered over several time levels, the method reduces the indeterminacy of the retrieval problem. (ii) Since the variational formulation is used, it is easy to incorporate other non–Doppler radar information, such as mass continuity as a weak constraint, or surface-wind observations, into the retrieval

Corresponding author address: Dr. Jidong Gao, Center for Analysis and Prediction of Storms, Sarkey's Energy Center, Suite 1110, 100 East Boyd, Norman, OK 73019.
E-mail: jdgao@ou.edu

procedure. (iii) Since the SA method only uses the conservation equation(s) for reflectivity and/or radial velocity, the boundary conditions are readily available. In contrast, the full adjoint method uses the complete set of equations where the boundary conditions involve unobserved variables (e.g., the cross-beam winds, temperature, etc.) (Sun et al. 1991).

The original SA method was designed for application in 2D horizontal planes, and the 3D mass continuity equation was not necessarily satisfied. Because the SA method neglects the observed vertical component of radial velocity, the retrievals may not work well for observations at high-elevation angles.

To avoid the above shortcomings, the original 2D version of the SA method is extended here to three dimensions. As such, all three wind components are retrieved in a dynamically consistent manner, using the entire volume of data. It is also easy to combine other 3D constraints, such as mass continuity in either weak or strong form. This paper presents a 3D version of the SA method and tests it with an idealized dataset.

This paper is organized as follows. In section 2, the 3D SA method is introduced; in section 3, the new SA method is tested with a set of idealized data sampled from a simulated supercell storm for which the true wind field is known; a summary and concluding remarks are given in section 4.

2. Description of methodology

Variational analysis is a procedure that minimizes a cost function, J, defined here to be the sum of squared errors due to the misfit between observations and analyses subject to certain constraints. Each constraint is weighted by a factor that accounts for its presumed accuracy. Different forms of J can be considered, and each of them will give a different result for the best-fit model solution.

The variational method makes use of the derivative of J with respect to the analysis variables, and thus J must be differentiable. The new SA method described herein retrieves the 3D time mean (over the retrieval period) wind vector (u_m, v_m, w_m) from single-Doppler observed radial velocity (V_r^{ob}) and/or reflectivity (η^{ob}) during a short time period (usually several minutes). The cost function that we use is defined as follows:

$$J = J_\eta + J_{V_{rm}} + J_B + J_D + J_S, \tag{1}$$

where the first term,

$$J_\eta = \frac{1}{2}\sum_{ijkn} W_\eta(\eta - \eta^{ob})^2, \tag{2}$$

defines the distance between predicted and observed tracer (either reflectivity or radial wind), that is, η and η^{ob}. The summation is over all gridpoint (i, j, and k) indices and time levels (n). Here η is ''predicted'' by a simplified three-dimensional advection equation:

$$\frac{\partial\eta}{\partial t} + u_m\frac{\partial\eta}{\partial x} + v_m\frac{\partial\eta}{\partial y} + w_m\frac{\partial\eta}{\partial z} - k_h\nabla_h^2\eta - k_v\nabla_v^2\eta = F_m. \tag{3a}$$

The boundary and initial values of (3a) are given by

$$\eta(t, x, y, z) = \eta^{ob}(t, x, y, z), \quad \text{at the boundary, and}$$
$$\eta(0, x, y, z) = \eta^{ob}(0, x, y, z), \tag{3b}$$

where the superscript ''ob'' denotes observed values, and u_m, v_m, and w_m are temporal mean velocities to be retrieved. The coefficients of eddy viscosity, k_h and k_v, are assumed to be unknown constants and will be retrieved. Here, F_m is a time-mean source also to be retrieved and includes effects such as the centrifugal and the pressure gradient forces if the tracer is radial velocity, or the sources and sinks of hydrometeors in association with microphysical processes and effect of terminal velocity if the tracer is reflectivity.

The second term $J_{V_{rm}}$ defines the distance between the analyzed (V_{rm}) and observed temporal mean radial wind (V_{rm}^{ob}):

$$J_{V_{rm}} = \frac{1}{2}\sum_{ijk} W_{rm}(V_{rm} - V_{rm}^{ob})^2. \tag{4}$$

Here, V_{rm}^{ob} is obtained by averaging V_r^{ob} over the retrieval time period, and V_{rm} has the following relationship with u_m, v_m, and w_m:

$$V_{rm} = \frac{xu_m + yv_m + zw_m}{r}, \tag{5}$$

where r is radial distance from the radar.

The other terms in the cost function have the following definitions:

$$J_B = \frac{1}{2}\left[\sum_{ijk} W_{ub}(u_m - u_b)^2 + \sum_{ijk} W_{vb}(v_m - v_b)^2 + \sum_{ijk} W_{wb}(w_m - w_b)^2\right], \tag{6}$$

$$J_D = \frac{1}{2}\sum_{ijk} W_D D^2, \quad \text{and} \tag{7}$$

$$J_S = \frac{1}{2}\left[\sum_{ijk} W_{us}(\nabla^2 u)^2 + \sum_{ijk} W_{vs}(\nabla^2 v)^2 + \sum_{ijk} W_{ws}(\nabla^2 w)^2\right]. \tag{8}$$

Here, J_B measures the fit of the variational analysis to the background field, and J_D imposes a weak anelastic mass continuity constraint on the analyzed wind field, where

$$D \equiv \frac{\partial\overline{\rho}u}{\partial x} + \frac{\partial\overline{\rho}v}{\partial y} + \frac{\partial\overline{\rho}w}{\partial z}, \tag{9}$$

and $\overline{\rho}$ is the mean air density profile and is a function of height only. The last term in the cost function, J_s, is a spatial smoothness constraint.

In the above expressions, the W's are weighting coefficients that depend on the error statistics of the constraint and are chosen empirically in this paper. In general, these coefficients should be matrices proportional to the inverse of the error covariance matrices of the associated terms in the cost function. In storm-scale data assimilation, especially for radar data, these error covariances are usually difficult to obtain. One of the major challenges of variational data assimilation is the statistical estimation of W. For our purposes, these coefficients are chosen based on both the estimated standard deviation of observed radial wind and the perceived relative importance of each term through numerical tests. Experience with the test cases presented herein suggests that the solutions obtained are not very sensitive to the precise values of W, and W can be treated as tuning parameters (Hoffman 1984). The analysis changes by only a small amount when a particular W is halved or doubled.

To solve the above variational problem by direct minimization, we need to derive the gradient of the cost function with respect to the control variables (u_m, v_m, w_m, F_m, k_h, and k_v). Taking the variation of J with respect to u_m, v_m, w_m, F_m, k_h, and k_v, we obtain the components of the gradient of J as follows:

$$\left(\frac{\partial J}{\partial u_m}\right)_{ijk} = \sum_n \left(\eta^* \frac{\partial \eta}{\partial x}\right) + W_{rn}\frac{x}{r}(V_{rm} - V_{rm}^{\text{ob}}) + W_{ub}(u_m - u_b) - W_D\overline{\rho}\partial D/\partial x + W_{su}\nabla^2(\nabla^2 u_m), \quad (10)$$

$$\left(\frac{\partial J}{\partial v_m}\right)_{ijk} = \sum_n \left(\eta^* \frac{\partial \eta}{\partial y}\right) + W_{rm}\frac{y}{r}(V_{rm} - V_{rm}^{\text{ob}}) + W_{vb}(v_m - v_b) - W_D\overline{\rho}\partial D/\partial y + W_{sv}\nabla^2(\nabla^2 v_m), \quad (11)$$

$$\left(\frac{\partial J}{\partial w_m}\right)_{ijk} = \sum_n \left(\eta^* \frac{\partial \eta}{\partial z}\right) + W_{rm}\frac{z}{r}(V_{rm} - V_{rm}^{\text{ob}}) + W_{wb}(w_m - w_b) - W_D\overline{\rho}(\partial D/\partial z) + W_{sw}\nabla^2(\nabla^2 w_m), \quad (12)$$

$$\left(\frac{\partial J}{\partial F_m}\right)_{ijk} = \sum_n (\eta^*)dt, \quad (13)$$

$$\left(\frac{\partial J}{\partial k_H}\right) = \sum_{ijkn} (\eta^* \nabla_h^2 \eta)dt, \quad \text{and} \quad (14)$$

$$\left(\frac{\partial J}{\partial k_v}\right) = \sum_{ijkn} (\eta^* \nabla_v^2 \eta)dt, \quad (15)$$

where η^* is the solution of the following associated adjoint problem:

$$-\frac{\partial \eta^*}{\partial t} - \frac{\partial (u_m \eta^*)}{\partial x} - \frac{\partial (v_m \eta^*)}{\partial y} - \frac{\partial (w_m \eta^*)}{\partial z} - k_h \nabla_h^2 \eta^* - k_v \nabla_v^2 \eta^* = W_\eta(\eta - \eta^{\text{ob}}). \quad (16a)$$

The boundary and initial values of (16a) are given by

$$\eta^*(t, x, y, z) = 0, \quad \text{at the boundary, and}$$
$$\eta^*(T, x, y, z) = 0, \quad (16b)$$

where T is the time period of integration. In the above derivation, the commutation formula

$$\sum \alpha \nabla \beta = -\sum \beta \nabla \alpha \quad (17)$$

of the finite-difference analog is used (Sasaki 1970). (Note: when building computer code, the derivations above are performed using the equivalent finite-difference analogs. For clarity, we write them here in their continuous form.)

After the gradients of the cost function are obtained, the data retrieval problem can be solved via the following procedure.

1) Choose a first guess for the control vector $\mathbf{Z} = (u_m, v_m, w_m, F_m, k_h, \text{and } k_v)$ and integrate the advection equation (3a) with (3b) forward in time from $t = 0$ to T. Store the computed field.
2) Calculate the cost function using Eqs. (1), (2), (4), (6), (7), and (8) and the fields obtained from step 1.
3) Integrate the adjoint equation (16a) backward with (16b) in time from $t = T$ to 0, and calculate the gradients ($\partial J/\partial u_m$, $\partial J/\partial v_m$, $\partial J/\partial w_m$, $\partial J/\partial F_m$, $\partial J/\partial k_h$, and $\partial J/\partial k_v$) according to Eqs. (10)–(15).
4) Use a conjugate gradient or quasi-Newton minimization algorithm (Navon and Legler 1987) to obtain updated values of the control variables,

$$Z_{ijk}^{(n)} = Z_{ijk}^{(n-1)} + \alpha f\left(\frac{\partial J}{\partial Z}\right)_{ijk}, \quad (18)$$

where n is the number of iterations, α is the optimal step size obtained by the ''line-search'' process in optimal control theory (Gill et al. 1981), and $f(\partial J/\partial Z)_{ijk}$ is the optimal descent direction obtained by combining the gradients from several former iterations.
5) Check whether the optimal solution has been found by computing the norm of the gradients or the value of J to see if they are less than a prescribed tolerance. If the criteria are satisfied, stop iterating and output the optimal control vector (u_m, v_m, w_m, F_m, k_h, and k_v).
6) If the convergence criterion is not satisfied, steps 2 through 5 are repeated using updated values of (u_m, v_m, w_m, F_m, k_h, and k_v) as the new guess. The iteration process is continued until a suitable converged solution is found.

With the above variational method, the fall speed of precipitation has to be taken into account. For radar scans at nonzero elevation angles, the fall speed contributes to the Doppler estimate of radial velocity. Thus, the observations of radial velocity are adjusted to remove this contribution using

$$v_r = v_r' + w_t \sin\theta, \tag{19a}$$

where v_r is the air radial velocity, v_r' is the target radial velocity, w_t is the terminal velocity of precipitation, and θ is the elevation angle (0° is horizontal). Here an empirical relationship is used between the reflectivity factor, Z, and raindrop terminal fall velocity (Foote and duToit 1969; Atlas et al. 1973):

$$w_t = 2.65\left(\frac{\rho_0}{\rho}\right)Z^{0.114}, \tag{19b}$$

where ρ is the air density and ρ_0 is its surface value.

3. Tests with simulated radar data

a. Experiment design

To evaluate the performance of our SA method, we utilize a set of numerical model simulated single–Doppler radar data. This strategy is often called Observation System Simulation Experiments (OSSE). A well-documented tornadic supercell storm that occurred near Del City, Oklahoma, on 20 May 1977 is used for the numerical experiments. This storm has been studied extensively using both multiple-Doppler radar analysis and numerical simulation. For details on storm morphology and evolution, refer to Ray et al. (1981), Klemp et al. (1981), and Klemp and Rotunno (1983).

The Advanced Regional Prediction System (ARPS; Xue et al. 1995) is used here to perform a 2-h simulation of the Del City storm. The simulation starts from a thermal bubble placed in a horizontally homogeneous base state specified from the sounding used in Klemp et al. (1981). As in Klemp et al. (1981), a mean storm speed ($U = 3$ m s^{-1}, $V = 14$ m s^{-1}) is subtracted from the sounding to keep the right-moving storm near the center of the model domain.

The model grid comprises $67 \times 67 \times 35$ grid points with a uniform grid interval of 1 km in the horizontal and 0.5 km in the vertical. The physical domain size is therefore $64 \times 64 \times 16$ km^3. The center of the storm-initiating disturbance is located at $x = 48$ km, $y = 16$ km, and $z = 1.5$ km, with the origin (0, 0, 0) at the lower left corner of the grid. The radius of the bubble is 10 km in both the x and y directions and 1.5 km in the vertical. The magnitude of the thermal perturbation is 4°. The Kessler (1969) warm rain microphysics option is used together with a 1.5-order turbulent kinetic energy subgrid turbulence parameterization. Open boundary conditions are used at the lateral boundaries, while an upper-level Rayleigh damping layer is included to reduce wave reflection from the top of the model.

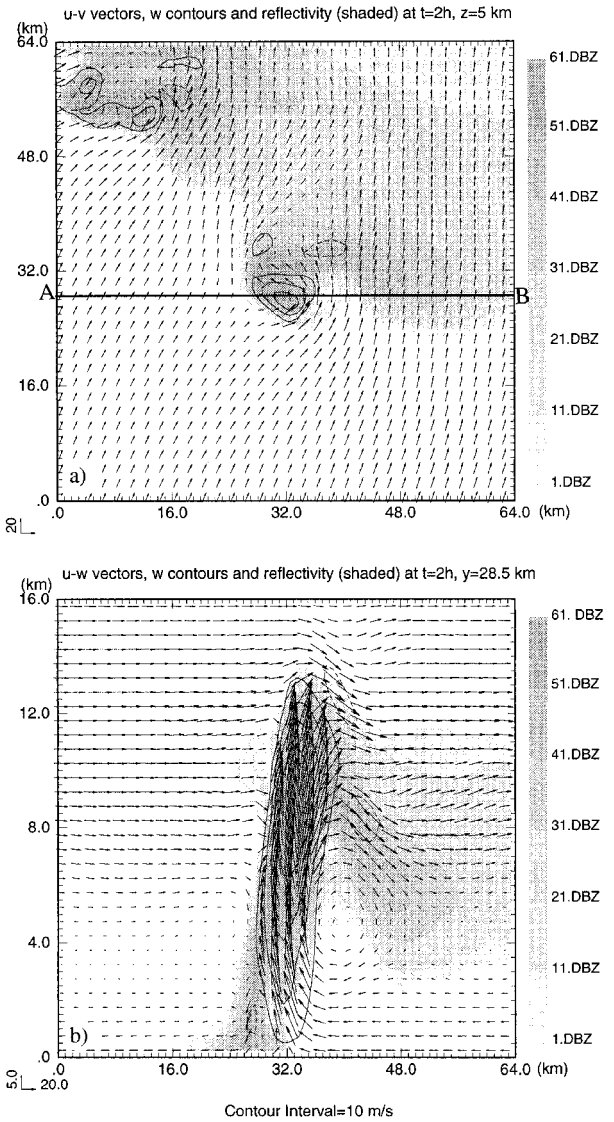

FIG. 1. The ARPS model simulated wind vectors, vertical velocity w (contours), and simulated reflectivity fields (shaded) of the 20 May 1977 supercell storm at 2 h. (a) Horizontal cross section at $z = 5$ km. (b) Vertical cross section at $y = 28.5$ km, [i.e., through line A–B in (a)].

By 2 h into the simulation, the initial storm has undergone a splitting process (Klemp and Wilhelmson 1978), with the right mover remaining near the center of the domain and the left mover propagating to the northwest corner of the domain. Figure 1 shows horizontal and vertical cross sections of storm-relative wind, vertical velocity (vertical section is plotted through line A–B in Fig. 1a), and reflectivity at 2 h. A strong rotating updraft (with maximum vertical velocity exceeding 34 m s^{-1}) and associated low-level downdraft are evident near the center of the domain, while the left mover is about to exit the domain. Downstream of the overshooting updraft at the tropopause level are downward returning flows that exhibit gravitational oscillations (Fig.

TABLE 1. List of experiments with a simulated dataset.

Experiments	First guess	Error of radial velocity	Horizontal wind (V_H)			Vertical wind (w)		
			rms	rre	CC	rms	rre	CC
CNTL1	Zero	No error	3.884	0.205	0.980	1.596	0.742	0.691
CNTL2	A sounding	No error	3.719	0.196	0.981	1.492	0.694	0.721
ERR1	A sounding	60%	3.724	0.196	0.981	1.568	0.729	0.682
ERR2	A sounding	100%	3.733	0.197	0.980	1.600	0.744	0.666

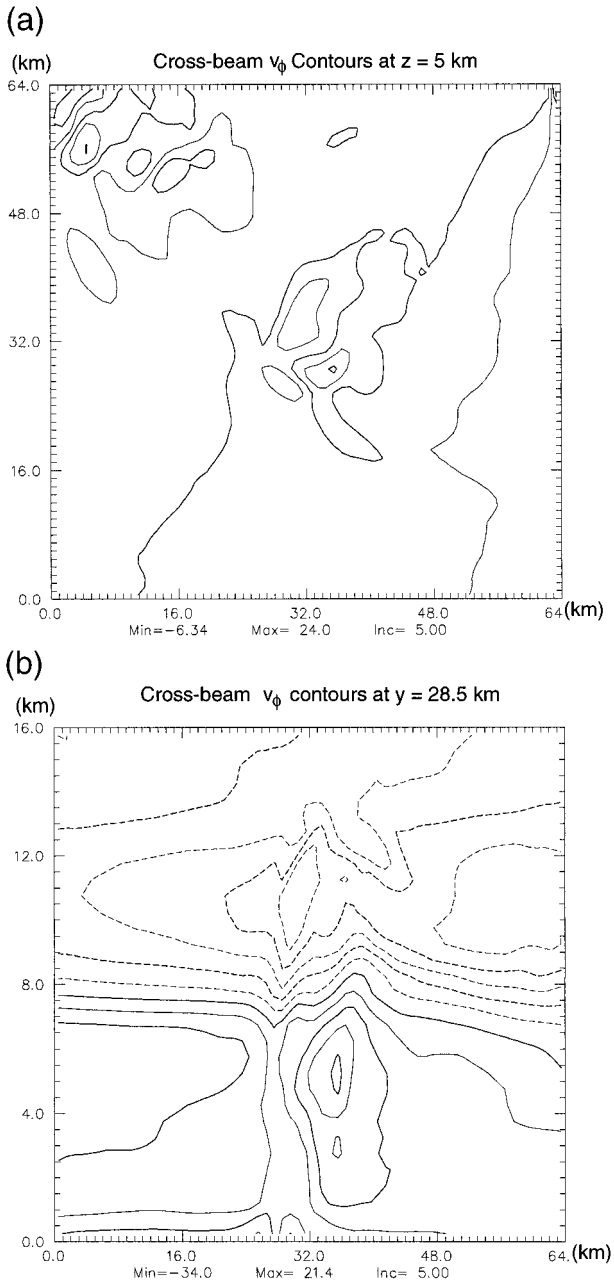

FIG. 2. The contours of the ARPS model simulated cross-beam wind component v_ϕ. (a) Horizontal cross section at $z = 5$ km. (b) Vertical cross section at $y = 28.5$ km.

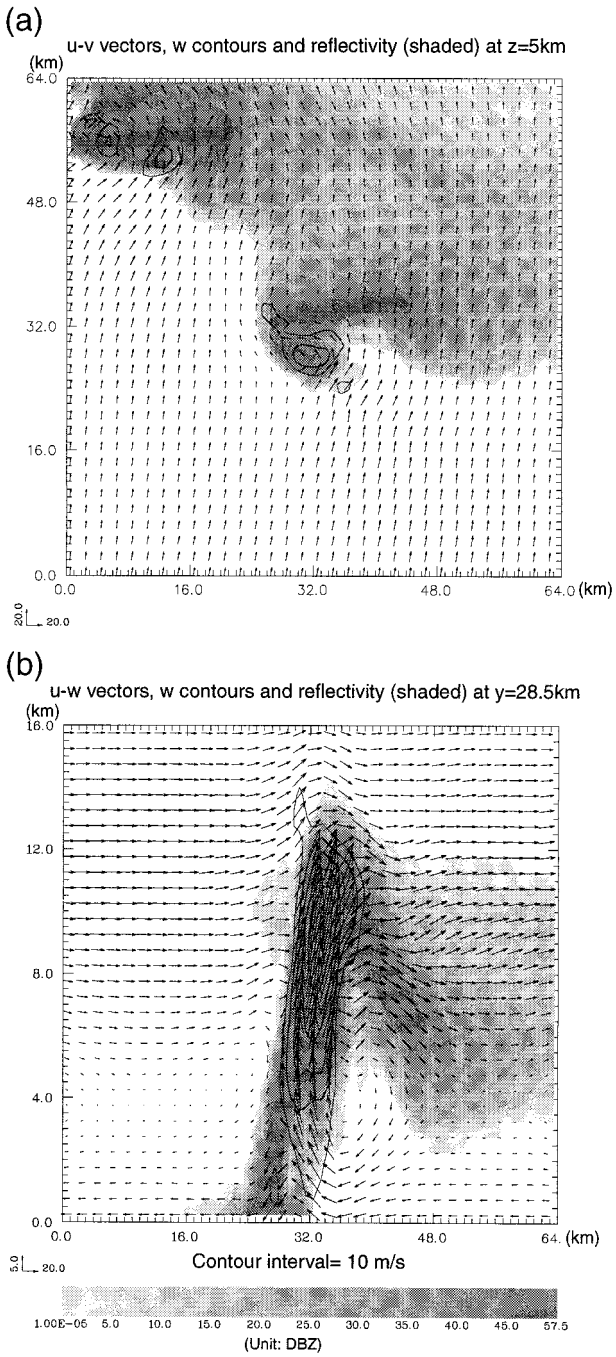

FIG. 3. The retrieved wind vectors and the contours of vertical velocity w in CNTL1. Others are the same as in Fig 1. The first-guess wind is zero.

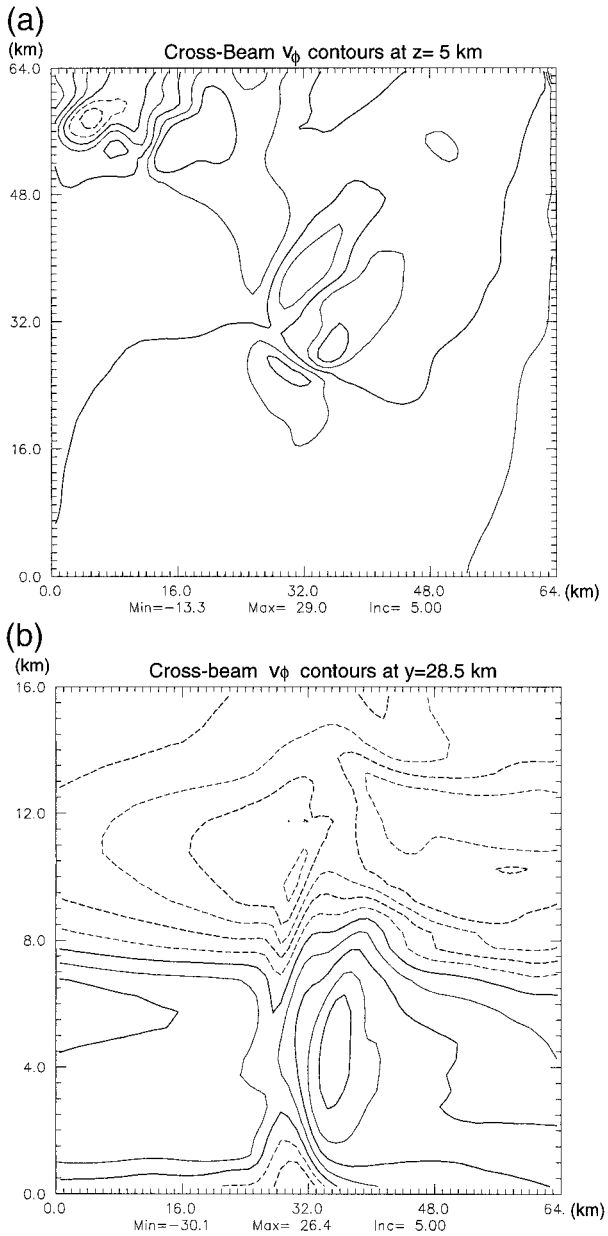

FIG. 4. The contours of retrieved cross-beam wind component v_ϕ in CNTL1. Others are the same as in Fig. 2.

1b). The evolution of the simulated storm is qualitatively similar to that described by Klemp et al. (1981), and by 2 h, it has attained a structure typical of mature supercell storms.

The simulated 3D convective-scale wind field at 2 h is sampled by a single pseudo Doppler radar, located at the (64, 64) grid point, that is, the northeastern corner in Fig. 1a at ground level. The radial wind components are synthesized to obtain radial velocities at each model grid point according to Eq. (5). The elapsed times for the volume scans of the pseudoradar are neglected, and thus we assume that the radial wind observations are simultaneous. These simulated radial velocity data at time levels 7050 and 7350 s are used as the tracer field in Eq. (3a). This time interval is similar to a time period of each volume scan of NEXRAD. The contours of horizontal cross-beam component v_ϕ of simulated wind at 2 h are plotted in Fig. 2 for the future comparison. To minimize the ''identical twin'' problem of OSSE experiments, we contaminate the pseudoradar data with random errors of different magnitudes in two of the experiments (see below). When radar data are used to initialize a numerical weather prediction model, a complete description of the wind and other meteorological variables is needed in the entire model domain. Even for diagnostic studies, consistent analysis outside the radar data areas is also desirable. Here the rawinsonde data near the storm location are incorporated into the cost function as a background environment.

The parameter settings used for the retrievals are $W_{rm} = 1$, $W_{ub} = W_{vb} = 10^{-2}$, $W_{wb} = 0.$, $W_D = 1/(0.5 \times 10^{-3})^2$, and $W_{us} = W_{vs} = W_{ws} = 0.5 \times 10^{-3}$. These values are chosen so that the constraints have proper orders of magnitude after being multiplied by the coefficients. These parameters also indicate the relative importance of each term in the cost function.

To measure the accuracy of the single-Doppler radar retrievals, we calculate the following rms error and relative rms error (rre) of the horizontal winds,

$$\text{rmsv} = \sqrt{\frac{\sum_{i=1}^{N} (u - u_{\text{ref}})_i^2 + \sum_{i=1}^{N} (v - v_{\text{ref}})_i^2}{2N}}, \quad (20)$$

$$\text{rrev} = \sqrt{\frac{\sum_{i=1}^{N} (u - u_{\text{ref}})_i^2 + \sum_{i=1}^{N} (v - v_{\text{ref}})_i^2}{\sum_{i=1}^{N} (u_{\text{ref}})_i^2 + \sum_{i=1}^{N} (v_{\text{ref}})_i^2}}, \quad (21)$$

and the rms error and relative rms error of the vertical velocities,

$$\text{rmsw} = \sqrt{\frac{\sum_{i=1}^{N} (w - w_{\text{ref}})_i^2}{N}}, \quad (22)$$

$$\text{rrew} = \sqrt{\frac{\sum_{i=1}^{N} (w - w_{\text{ref}})_i^2}{\sum_{i=1}^{N} (w_{\text{ref}})_i^2}}. \quad (23)$$

Here, N represents the total number of grid points, and the subscript ''ref'' stands for the reference or actual field sampled from the ARPS model solution. In addition, the correlation coefficients of horizontal and vertical winds between the retrieved fields (u, v, and w) and reference fields (u_{ref}, v_{ref}, and w_{ref}) also are calculated for each experiment.

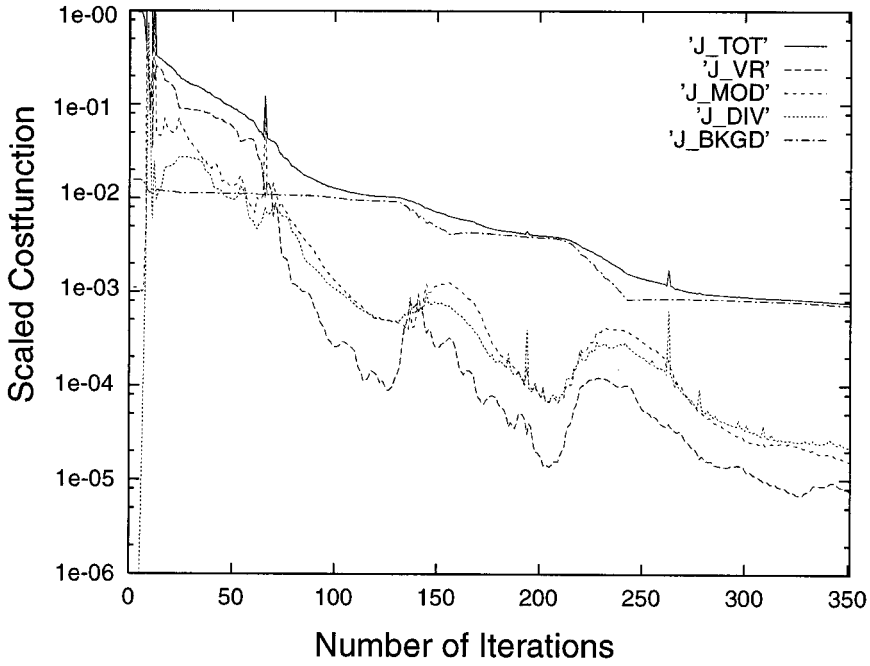

FIG. 5. The scaled total cost function (J_k/J_0) and contribution of each constraint as a function of the number of iterations. The first-guess wind is zero. J_TOT stands for the total cost function; J_VR, J_MOD, J_DIV, and J_BKGD stand for contribution from the mean radial velocity, the simple conservation equation, the mass continuity, and background constraints, respectively.

b. Results of retrievals

In this section, we present the results from the set of OSSE experiments outlined in the previous section. The analysis domain is the same as the ARPS integration domain described earlier, and the experiments are listed in Table 1. There are two control runs (CNTL1 and CNTL2), and two experiments (ERR1 and ERR2) are designed to test the sensitivity of the retrievals to imposed error.

We first discuss the number of iterations needed to minimize *J*. Generally speaking, the optimal number is case dependent, and is also a function of the preconditioning and minimization method used. In practice, the appropriate number of iterations can be estimated by examining the behavior of the cost function, that is, the minimization process can be stopped when the change in the cost function becomes small (explained below). To obtain a reasonably converged solution, 350 iterations are used in all experiments.

We examine first CNTL1, for which all constraints discussed in section 2 are included. The first guesses for all the wind components and the forcing term of the simplified equation are set to zero, and the first guess for the horizontal and vertical diffusion coefficients are set to 200 m s^{-2}. The retrieval results are presented in Figs. 3 and 4. Comparing Fig. 3 with the true fields in Fig. 1, all features in the horizontal winds, that is, the curvature around the rotating updraft as well as the convergence, are well retrieved (Fig. 3a). The general structure of the updraft is well retrieved at all levels, and a downdraft in the western part of model domain is present. Oscillations downstream of the main updraft top due to gravity waves are also obvious in Fig. 3b. The relative rms errors are small for the horizontal wind (0.205) and, although they are not small for vertical velocity (0.742), the correlation coefficient (0.691) and the general flow structure are quite reasonable (Fig. 3). This is so because most of the error is in the amplitude, while the phase error is relatively small, and the retrieved vertical motion is weaker than the true one. To clearly show how much of the unobserved wind field is retrieved, the contours of cross-beam component v_ϕ are plotted in Fig. 4. The major pattern near the storm center agrees well with the true one in Fig. 2, while the cross-beam component v_ϕ of the left-moving storm is not well retrieved. The contours of cross-beam component v_θ (not shown here) in the elevation direction are almost same as the *w* contours.

To further examine in detail the quality of this retrieval, the variation of the cost function and the gradient norm for each constraint (except for smoothness, which is smaller than the others) with the number of iterations, are presented in Figs. 5 and 6. It is clear that the background constraint accounts for the largest part in the total cost function, while the other constraints, including the simple conservation equation, mean radial velocity, and mass continuity constraints, have about the same order-of-magnitude contributions to the total cost func-

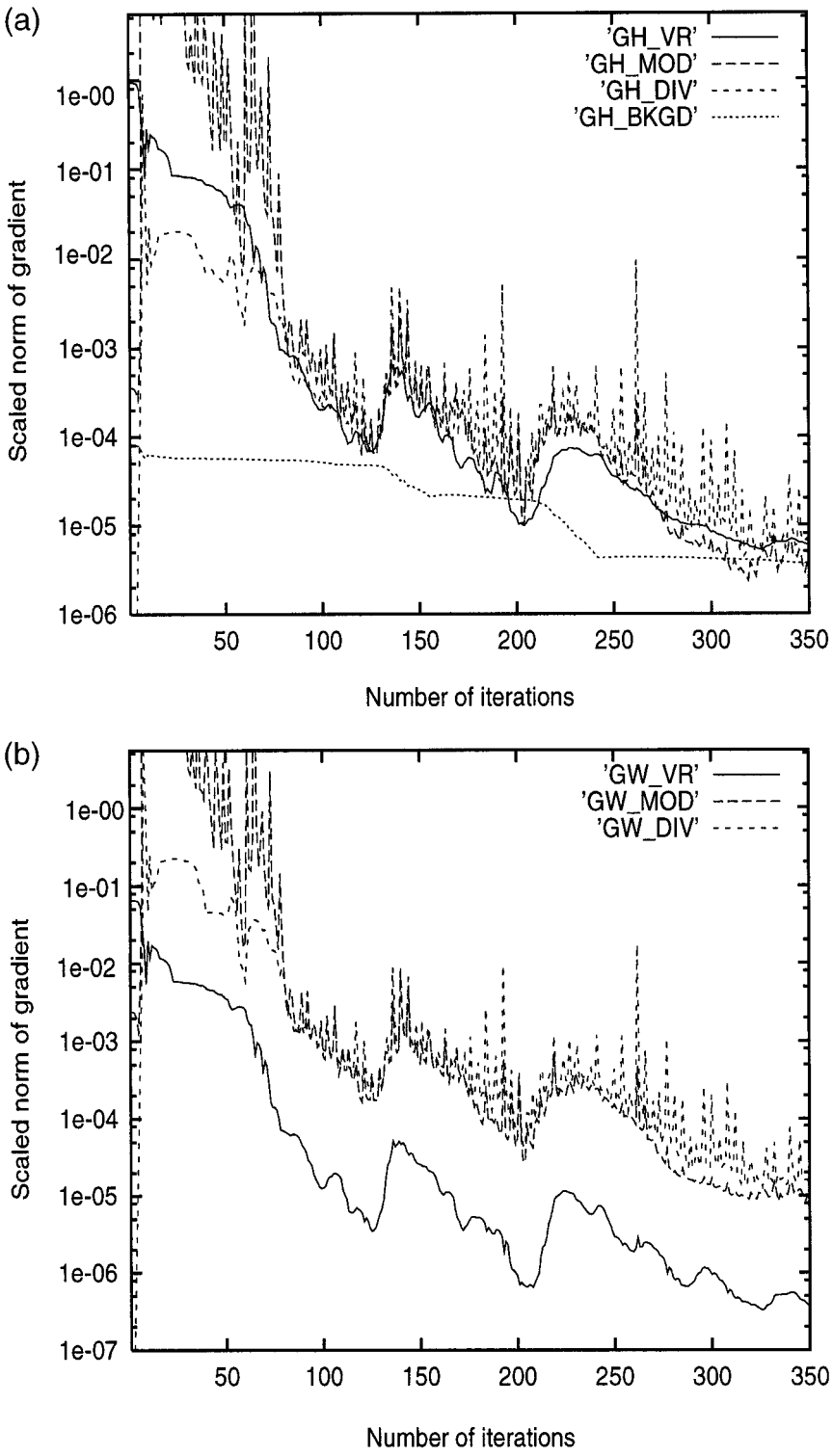

FIG. 6. The scaled norm of gradient of each constraint as a function of the number of iterations. (a) The contribution to horizontal wind. (b) The contribution to vertical velocity. The first-guess wind is zero. GH_VR, GH_MOD, GH_DIV, and GH_BKGD stand for contribution from the mean radial velocity, the simple conservation equation, the mass continuity, and background constraints to the retrieval of horizontal wind, respectively. GW_VR, GW_MOD, and GW_DIV stand for contribution from the mean radial velocity, the simple conservation equation, and the mass continuity constraints to the retrieval of vertical velocity, respectively.

tion. This indicates that the distance between the retrieval and the uniform background (given by a single sounding) remains large, and therefore the background constraint does not dominate the analysis field. The cost functions for the other constraints are reduced by more than four orders of magnitude during the iterations.

Figure 6a shows that the norm of the gradient of the background constraint is smallest among all constraints for nearly all iterations (note that the background constraint does not have any contribution to the retrieval of vertical velocity because the background w is zero and is not used as a constraint). Comparing Fig. 6a with Fig. 6b, the contribution of mean radial wind constraint to the horizontal wind retrieval is of the same order as the other constraints except for the background, while the contribution of the mean wind to the vertical velocity is significantly less than that of the other constraints. This is because Doppler radars usually operate at low-elevation angles, with the horizontal winds much better observed than vertical winds. Hence, the cost function corresponding to the mean radial wind constraint is more sensitive to horizontal winds than to vertical winds, and therefore the horizontal wind component is easier to retrieve with the help of this constraint. The contribution of vertical velocity to the observed radial velocities is, however, relatively small due to the small elevation angles; thus the retrieved w tends to be less accurate. Comparing Fig. 6a with Fig. 6b, the conservation equation and mass continuity constraint play about the same role for the retrieval of both horizontal and vertical winds.

Experiment CNTL1 gives a satisfactory wind retrieval, but the variations of both the cost function and the norm of the gradient show large fluctuations with the number of iterations, because the first guesses for all control variables are zero. The distance between the minimum (optimal analysis) and the first guesses is therefore so great that it is difficult to obtain a global minimum for the cost function. In CNTL2, we perform an experiment that is exactly the same as CNTL1, except that the first guesses for the control variables are set to their background values from the single environmental sounding.

Comparing Fig. 7 with Fig. 3, little difference can be perceived, indicating in both cases that the minimization of the cost function to the global minimum is reasonably well achieved. Figure 8 shows that the total cost function (solid line) starts to level off after 100 iterations. From 150 iterations on, the curve of total cost function becomes essentially horizontal. This indicates that the global minimum (or optimal analysis) could be obtained in a relatively small number of iterations, say about 100–150. The fluctuation in cost function and gradient norm for each constraint are much smaller, so that the minimization of the cost function is easier to achieve than in CNTL1. For operational data assimilation, the number of iterations may have to be smaller (usually 50). Fortunately, much better

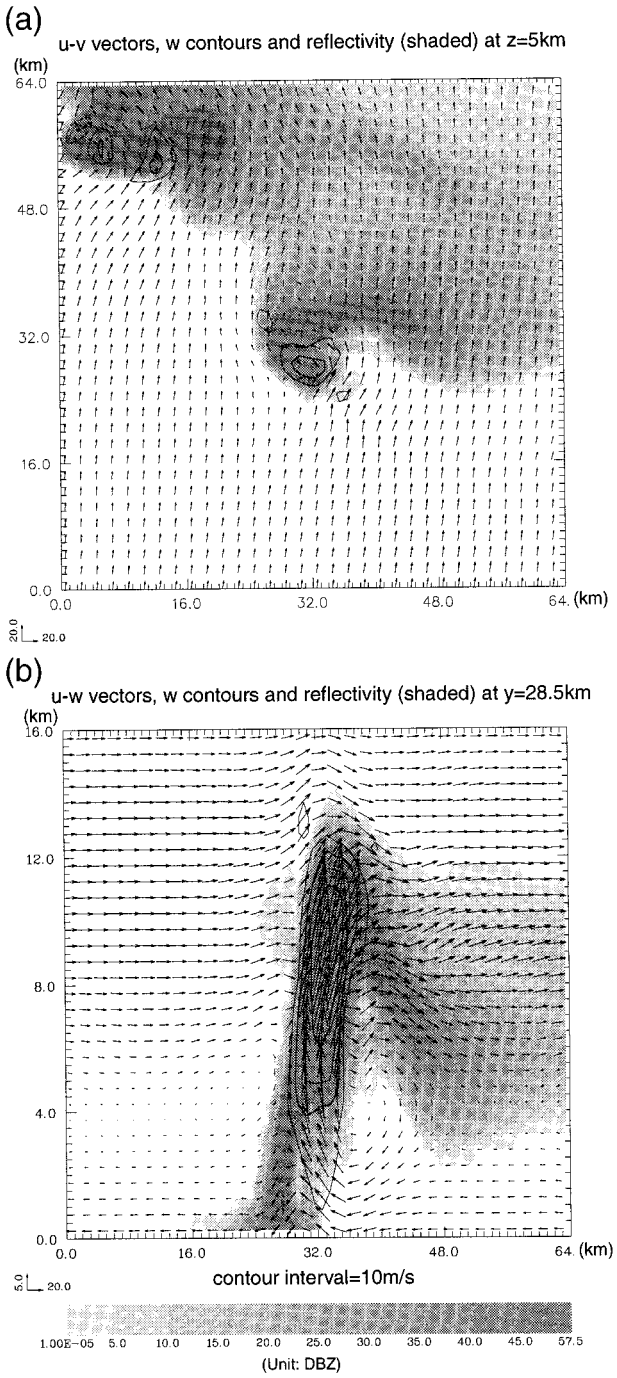

FIG. 7. As in Fig. 3, but for CNTL2. The first guess is from a sounding.

first guesses from a previous model forecast or analysis using traditional observations are usually available, which should, as our results suggest, accelerate the minimization.

In reality, radial wind observations can contain large errors, especially of bias nature (e.g., ground clutter and

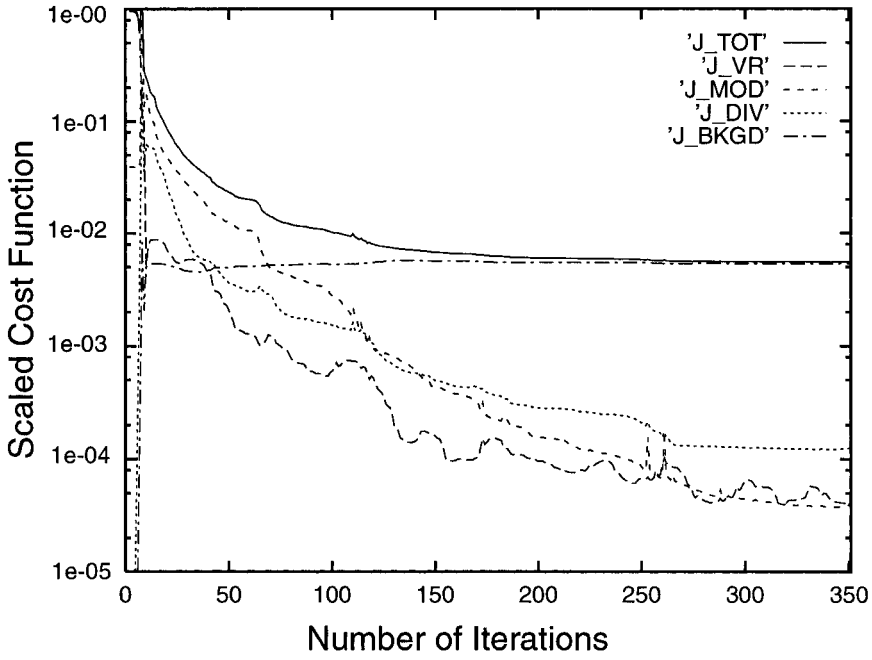

FIG. 8. As in Fig. 5, but for CNTL2. The first guess is from a sounding.

anomalous propagation). However, it is very difficult to account for such errors in detail. In our OSSE experiments, the simulated data are obtained from a model run (ARPS). When these data are used in the SA method (which is not based on the ARPS formulations), these are not identical twin experiments, and some systematic errors are already introduced to CNTL1 and CNTL2 because the simulated data are not produced by a forward model of the SA method.

In this section, we test the quality of the retrieved fields subject to random observational errors. Experiments ERR1 and ERR2 (Table 1) involve the addition of 60% and 100% random errors, respectively, to the radial wind observations. In other words, we use $V_r' = (1 + \alpha\varepsilon)V_r$ as the observations, where ε represents random numbers between -1 and $+1$, and α is 0.6 and 1.0, respectively.

When $\alpha = 0.6$, the relative rms error for the horizontal wind is not changed from that of CNTL2 (0.196 for both cases). However, the rms error of vertical velocity increases from 0.694 to 0.729, and the correlation coefficient decreases from 0.721 to 0.682. Thus, the vertical velocity is more sensitive to observational errors than the horizontal wind. Nevertheless, the general features of the 3D wind field are well retrieved (figure not shown).

When α is increased to 1.0, Fig. 10 shows that considerable noise exists in the retrieved horizontal and vertical wind fields. In spite of that, the general pattern of the flow remains rather similar to the pseudo observations. This example shows that the method is rather robust even for such large observational errors. The relative rms errors of the horizontal and vertical winds remain reasonably small (0.197 and 0.744), as in the other experiments.

4. Concluding remarks

The original SA method of Qiu and Xu (1992) was designed for application in independent 2D horizontal planes, and the 3D mass continuity conservation equation was not necessarily satisfied. The method neglects the observed vertical component of the radial wind, and the vertical velocity is not retrieved simultaneously. One way to obtain the vertical velocity is to apply the original SA method to a number of horizontal levels and then integrate the mass continuity conservation equation in the vertical direction. By doing so, the horizontal and vertical winds are derived in two separate steps and accuracy tends to be poor because the retrieved horizontal winds in each plane may not be consistent with each other.

In this paper, a new simple adjoint method that is capable of retrieving the full 3D wind field from single-Doppler observations of convective storms is proposed and tested. The new method incorporates, in a single cost function, a conservation equation for an observed variable (radial wind and/or reflectivity), along with constraints for the mean radial wind, anelastic mass continuity and the background fields, and smoothness (Gao et al. 1999a). By minimizing this cost function, an analysis with the desired fit to these constraints is obtained in a single analysis procedure. Furthermore, the method is flexible for incorporating additional types of data, for

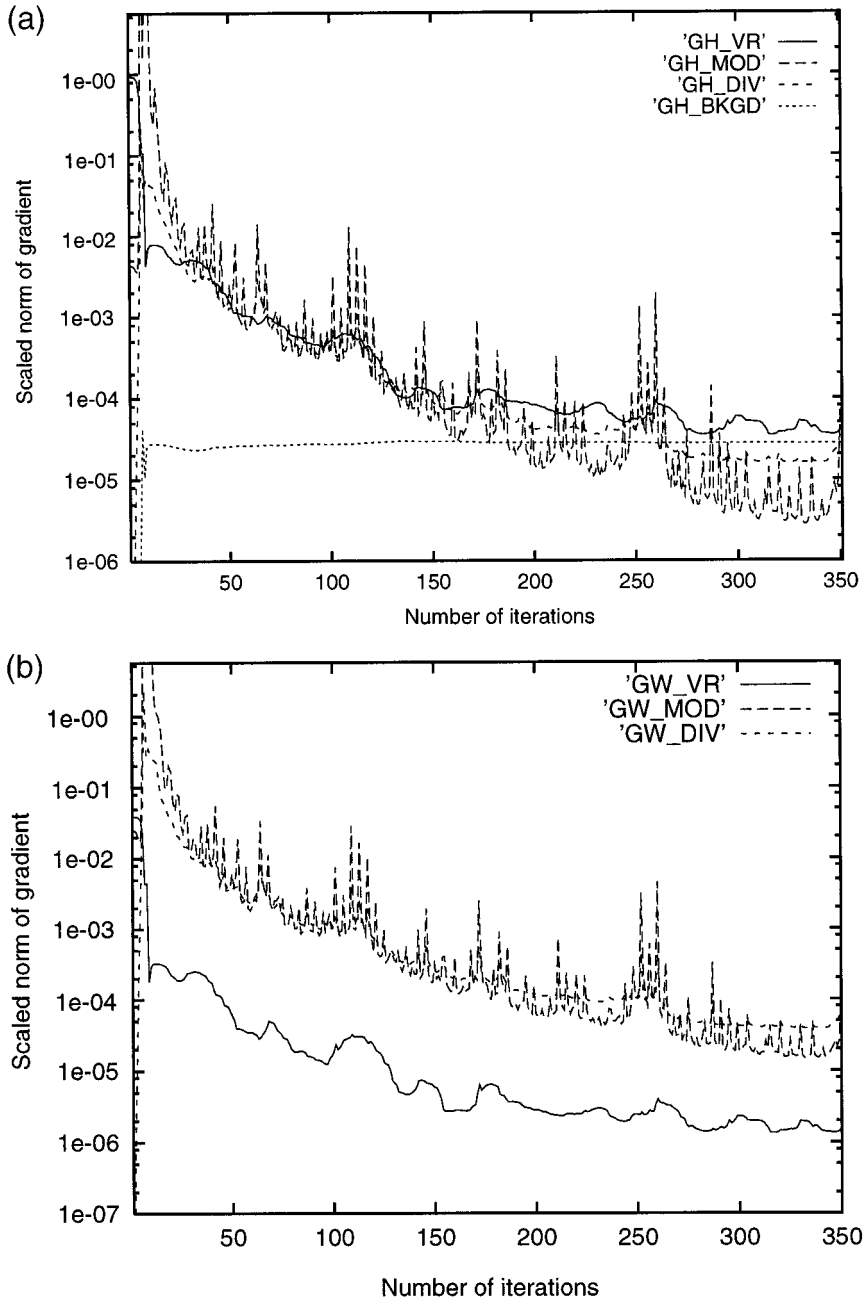

FIG. 9. As in Fig. 6, but for CNTL2. The first guess is from a sounding.

example, analyzed or forecast background fields and/or conventional observations (e.g., surface mesonet, upper-air sounding, and profiler data). Because the anelastic mass continuity equation is used as a weak constraint, no explicit integration of this equation occurs, and error accumulation associated with such integration is avoided. The method is robust enough to resist large random observational errors.

Although we have shown here, using only OSSE experiments, that the upgraded SA method has merit, the method should be tested with real data. An application of WSR-88D Doppler radar data gathered during the VORTEX95 field experiment project is under investigation, and preliminary results have shown promise (see Gao et al. 1999b). Further real data experiments of our method are being pursued and will be presented in a future paper.

Acknowledgments. This research was supported by NSF Grants ATM 91-20009 and ATM 99-09007 to the

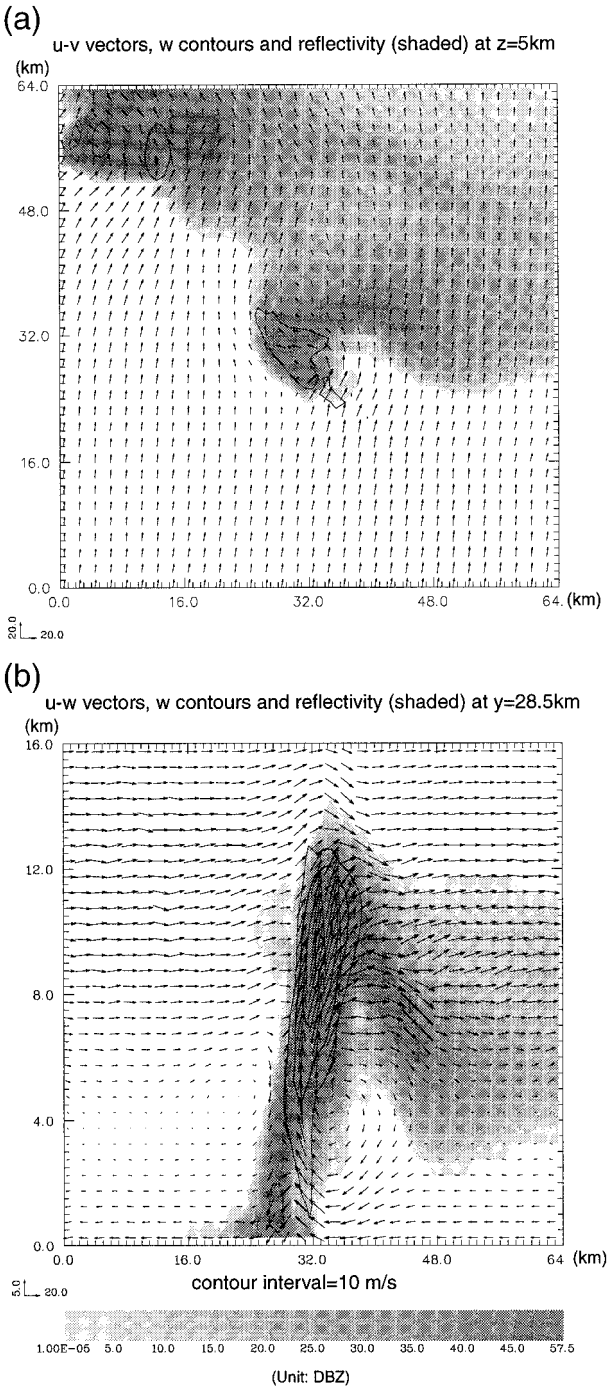

FIG. 10. As in Fig. 3, but for ERR2. The first guess is from a sounding.

Center for Analysis and Prediction of Storms (CAPS), and by the U.S. Department of Defense (Navy) Grant N00014-96-1-112, through the Coastal Meteorological Research Program. Graphic plots were generated by the ZXPLOT graphics package written by Ming Xue. Computations were performed on the Cray J90 of the Environmental Computing Applications System (ECAS) of the University of Oklahoma.

REFERENCES

Atlas, D., R. C. Srivastava, and R. S. Sekhon, 1973: Doppler radar characteristics of precipitation at vertical incidence. *Rev. Geophys. Space Phys.,* **11,** 1–35.

Foote, G. B., and P. S. duToit, 1969: Terminal velocity of raindrops aloft. *J. Appl. Meteor.,* **8,** 249–253.

Gao, J.-D., M. Xue, A. Shapiro, and K. K. Droegemeier, 1999a: A variational method for the analysis of three-dimensional wind fields from two Doppler radars. *Mon. Wea. Rev.,* **127,** 2128–2142.

——, ——, ——, Q. Xu, and K. K. Droegemeier, 1999b: Three-dimensional simple adjoint retrievals using WSR-88D radar data. Preprints, *Eighth Conf. on Mesoscale Processes,* Boulder, CO, Amer. Meteor. Soc., 338–340.

Gill, P. E., W. Murray, and M. H. Wright, 1981: *Practical Optimization.* Academic Press, 401 pp.

Hoffman, R. N., 1984: SASS wind ambiguity removal by direct minimization. Part II: Use of smoothness and dynamical constraints. *Mon. Wea. Rev.,* **112,** 1829–1852.

Kessler, E., 1969: *On the Distribution and Continuity of Water Substance in Atmospheric Circulation. Meteor. Monogr.,* No. 32, Amer. Meteor. Soc., 84 pp.

Klemp, J. B., and R. B. Wilhelmson, 1978: Simulations of right- and left-moving storms produced through storm splitting. *J. Atmos. Sci.,* **35,** 1097–1110.

——, and R. Rotunno, 1983: A study of the tornadic region within a supercell thunderstorm. *J. Atmos. Sci.,* **40,** 359–377.

——, R. B. Wilhelmson, and P. S. Ray, 1981: Observed and numerically simulated structure of a mature supercell thunderstorm. *J. Atmos. Sci.,* **38,** 1558–1580.

Laroche, S., and I. Zawadzki, 1994: A variational analysis method for retrieval of three-dimensional wind field from single–Doppler radar data. *J. Atmos. Sci.,* **51,** 2664–2682.

Liou, Y. C., T. Gal-Chen, and D. K. Lilly, 1991: Retrieval of winds, temperature, and pressure from single-Doppler radar and a numerical model. Preprints, *25th Int. Conf. on Radar Meteorology,* Paris, France, Amer. Meteor. Soc., 151–154.

Navon, I. M., and D. M. Legler, 1987: Conjugate-gradient methods for large-scale minimization in meteorology. *Mon. Wea. Rev.,* **115,** 1479–1502.

Qiu, C.-J., and Q. Xu, 1992: A simple adjoint method of wind analysis for single-Doppler data. *J. Atmos. Oceanic Technol.,* **9,** 588–598.

Ray, P. S., B. C. Johnson, K. W. Johnson, J. S. Bradberry, J. J. Stephens, K. K. Wagner, R. B. Wilhelmson, and J. B. Klemp, 1981: The morphology of several tornadic storms on 20 May 1977. *J. Atmos. Sci.,* **38,** 1643–1663.

Rinehart, R. E., 1979: Internal storm motions from a single non-Doppler weather radar. NCAR Tech. Note NCAR/TN-146+STR, 262 pp.

Sasaki, Y., 1970: Some basic formalisms in numerical variational analysis. *Mon. Wea. Rev.,* **98,** 875–883.

Shapiro, A., S. Ellis, and J. Shaw, 1995: Single-Doppler velocity retrievals with Phoenix II data: Clear air and microburst retrievals in the planetary boundary layer. *J. Atmos. Sci.,* **52,** 1265–1287.

Sun, J., and N. A. Crook, 1997: Dynamical and microphysical retrieval from Doppler radar observations using a cloud model and its adjoint. Part I: Model development and simulated data experiments. *J. Atmos. Sci.,* **54,** 1642–1661.

——, and ——, 1998: Dynamical and microphysical retrieval from Doppler radar observations using a cloud model and its adjoint. Part II: Retrieval experiments of an observed Florida convective storm. *J. Atmos. Sci.,* **55,** 1642–1661.

——, D. W. Flicker, and D. K. Lilly, 1991: Recovery of three-dimensional wind and temperature fields from simulated single–Doppler radar data. *J. Atmos. Sci.,* **48,** 876–890.

Tuttle, J. D., and J. B. Foote, 1990: Determination of the boundary layer airflow from a single Doppler radar. *J. Atmos. Oceanic Technol.,* **7,** 218–232.

Weygandt, S., A. Shapiro, and K. Droegemeier, 1995: Adaptation of a single-Doppler velocity retrieval for use on a deep-convection storm. Preprints, *27th Conf. on Radar Meteorology,* Vail, CO, Amer. Meteor. Soc., 264–266.

Xu, Q., and C. J. Qiu, 1994: Simple adjoint methods for single-Doppler wind analysis with a strong constraint of mass conservation. *J. Atmos. Oceanic Technol.,* **11,** 289–298.

——, and ——, 1995: Adjoint-method retrievals of low-altitude wind fields from single-Doppler reflectivity and radial-wind. *J. Atmos. Oceanic Technol.,* **12,** 1111–1119.

——, ——, and J.-X. Yu, 1994a: Adjoint-method retrievals of low-altitude wind fields from single-Doppler reflectivity measured during Phoenix-II. *J. Atmos. Oceanic Technol.,* **11,** 275–288.

——, ——, and ——, 1994b: Adjoint-method retrievals of low-altitude wind fields from single-Doppler wind data. *J. Atmos. Oceanic Technol.,* **11,** 579–585.

Xue, M., K. K. Droegemeier, and V. Wong, 2000: The Advanced Regional Prediction System (ARPS)—A multiscale nonhydrostatic atmospheric simulation and prediction tool. Part I: Model dynamics and verification. *Meteor. Atmos. Phys.,* in press.

Zhang, J., and T. Gal-Chen, 1996: Single-Doppler wind retrieval in the moving frame of reference. *J. Atmos. Sci.,* **53,** 2609–2623.